

Embodied AI-Enhanced IoMT Edge Computing: UAV Trajectory Optimization and Task Offloading with Mobility Prediction

Siqi Mu, Shuo Wen, Yang Lu, *Member, IEEE*, Ruihong Jiang, *Member, IEEE*, and Bo Ai, *Fellow, IEEE*

Abstract

Due to their inherent flexibility and autonomous operation, unmanned aerial vehicles (UAVs) have been widely used in Internet of Medical Things (IoMT) to provide real-time biomedical edge computing service for wireless body area network (WBAN) users. In this paper, considering the time-varying task criticality characteristics of diverse WBAN users and the dual mobility between WBAN users and UAV, we investigate the dynamic task offloading and UAV flight trajectory optimization problem to minimize the weighted average task completion time of all the WBAN users, under the constraint of UAV energy consumption. To tackle the problem, an embodied AI-enhanced IoMT edge computing framework is established. Specifically, we propose a novel hierarchical multi-scale Transformer-based user trajectory prediction model based on the users' historical trajectory traces captured by the embodied AI agent (i.e., UAV). Afterwards, a prediction-enhanced deep reinforcement learning (DRL) algorithm that integrates predicted users' mobility information is designed for intelligently optimizing UAV flight trajectory and task offloading decisions. Real-word movement traces and simulation results demonstrate the superiority of the proposed methods in comparison with the existing benchmarks.

S. Mu and S. Wen are with the School of Sports Engineering, Beijing Sport University, Beijing 100084, China (e-mail: musiqi@bsu.edu.cn).

Y. Lu is with the School of Computer and Information Technology, Beijing Jiaotong University, Beijing 100044, China (e-mail: yanglu@bjtu.edu.cn).

R. Jiang is with the State Key Laboratory of Networking and Switching Technology, Beijing University of Posts and Telecommunications, Beijing 100876, China (e-mail: rhjiang@bupt.edu.cn).

B. Ai are with the School of Electronics and Information Engineering, Beijing Jiaotong University, Beijing 100044, China (e-mail: boai@bjtu.edu.cn).

Corresponding author: Yang Lu.

Index Terms

IoMT, embodied AI, mobility prediction, hierarchical Transformer, DRL.

I. INTRODUCTION

A. Background and Prior Works

Recent advancements in Internet of Medical Things (IoMT) and artificial intelligence (AI), have made a significant contribution to sustainable digital health. Combining traditional medical equipments with IoT, IoMT provides ubiquitous in-home healthcare, and greatly alleviates public medical burdens and saves healthcare resources [1]. As the key components of IoMT, wireless body area networks (WBANs) deploy various low-power biosensors on numerous people. These heterogeneous biosensors sense various types of physiological data, including electrocardiogram (ECG), electroencephalogram (EEG), blood pressure (BP), body temperature etc., and transmit the data to an on-body sink node for further processing [2], [3]. WBANs have significantly facilitated pervasive health monitoring services and promoted real-time health assessment.

Despite these promising developments, the rapid population growth, especially the aged, and their medical tasks still overloads the healthcare infrastructure, and limits the development of IoMT [4]. Local sink nodes, such as mobile phones and laptops, cannot satisfy the latency requirements of the time-sensitive tasks for medical information analysis. The proliferation of mobile edge computing (MEC) is conceived as a promising paradigm for tackling such challenges [5]. By providing computation resources for the offloaded medical analysis tasks in proximity, MEC alleviates the burden on local devices and augments the capability of IoMT. The integration of IoMT and MEC has been envisioned as an effective approach for real-time healthcare service provision, especially during the COVID-19 pandemic [6], [7].

With the continuous increase in WBAN users, cellular infrastructure-based MEC, in which edge servers deployed at terrestrial base station, struggles to provide seamless connectivity and reliable computation [8]. Benefiting from its high mobility, flexible deployment capabilities and strong scalability, UAV-enabled MEC has gained widespread attention and become a research hotspot. Particularly, computation offloading and UAV flight trajectory in a MEC system are

jointly optimized to minimize the overall task delay of users [9], [10], or minimize the energy consumption of UAV [11]. By enabling UAV to simultaneously act as a relay and MEC server, [12] and [13] optimized the task offloading, bandwidth allocation, computation resource scheduling and UAV trajectory using successive convex approximation, such that maximizing the energy efficiency of users and UAV. Later in [14], a UAV enabled edge-cloud computing system was considered to augment the computation capability of the UAV. A delay minimization problem for edge-cloud cooperative offloading was investigated in this paper. However, these earlier studies have been conducted on the static scenarios without consideration on user mobility, which is unrealistic since user locations may change dynamically over time in practice. In addition, user mobility directly impacts UAV path planning and edge computing performance.

To tackle this problem, several studies focused on mobile users, where the user mobility model follows the random waypoint mobility model [15], reference point group mobility model [16], [17], or the Gauss-Markov mobility model [18], [19]. These models have been applied to derive the UAV coverage probability [15] or develop optimization algorithms on user association, power allocation, subchannel assignment, UAV positioning or trajectory design under various system objectives, such as maximizing system throughput [16], [17] or energy efficiency [18], [19]. However, in these ideal mobility models, the direction of user's movement tends to be uniformly distributed among left, right, forward and backward, which does not fully reflect the complexities and nuances of the real-world user movement [20]. Additionally, although user mobility patterns were considered, the algorithm designs in these works were based on the assumption that precise user locations are accessed by UAV in real time. Such an assumption is difficult to fulfill in practice, especially in urban environments or areas with significant obstructions. Even worse, the user location information reported to UAV may be outdated due to the fast movement of users, leading to suboptimal task offloading strategy and UAV path planning [21].

In view of these, a few researchers have made efforts to capture the time-varying uncertainty of user mobility with prediction models to improve the service quality of edge computing. [22] proposed a LSTM-based mobility prediction model, based on which a predictive service placement algorithm was designed to balance the latency performance and handover cost. In [23], the

authors developed a seq2seq user trajectory prediction model, alongside a deep reinforcement learning (DRL) algorithm for supporting offloading decisions and resource allocation in MEC, to minimize the average task latency of users. In spite of these innovative attempts, several challenges still remains. First, these existing studies on MEC with mobility prediction mainly focus on the communication connections between terrestrial base station and users, how to improve the edge computing performance in an air-ground system with dual mobility of UAV and ground users needs to be further investigated. Besides, inaccuracies in the existing trajectory prediction methods can result in suboptimal offloading decisions and UAV trajectory optimization, which will increase task completion time and UAV energy consumption. It is imperative to develop a more robust and predictive framework. Finally, few works on UAV-assisted MEC systems consider the time-varying criticality of computation tasks, which is a significant and indispensable feature for WBAN users. How to intelligently make offloading decisions based on the time-varying task characteristics is non-trivial.

B. Contributions

Motivated by the challenges and inspired by the advanced AI techniques, we propose an embodied AI-enhanced UAV edge computing framework in this work. Embodied AI, which emphasizes the physical objects embedded with intelligent system actively interact with and learn from their physical surroundings, has been shown a promising solution for dealing with this highly complex and dynamic scenario [24], [25]. Specifically, the proposed framework is comprised of two core modules, i.e., a hierarchical Transformer enabled user mobility prediction module and a DRL enabled UAV trajectory optimization and task offloading module. The embodied AI system embedded within UAV enables accurate mobility prediction and real-time strategy adaptation to dynamic environments. Equipped with the designed AI algorithms, the UAV embodied AI agent predicts user mobility based on the perceived historical information, and autonomously optimizes flight trajectory and makes intelligent task offloading decisions. The contributions of this work are summarized as follows:

- 1) Considering the time-varying task criticality characteristics of diverse WBAN users, we formulate a dynamic multi-stage task offloading and UAV flight trajectory optimization

problem, aiming at minimizing the weighted average task completion time of all the WBAN users, subject to the total energy consumption of the UAV.

- 2) To facilitate the optimization of flight trajectory and task offloading decisions for the UAV embodied AI agent, we propose a novel user trajectory prediction model based on a hierarchical multi-scale Transformer framework. Through the design of trajectory slice partitioning, embedding representation and the attention mechanism, the proposed model can capture the temporal dependencies of historical user trajectory on various time scales.
- 3) The original dynamic optimization problem is transformed into a Markov decision process (MDP) problem. Based on the designed state, action and reward function, a prediction-enhanced DRL algorithm that integrates predicted users' mobility information is developed for intelligent UAV trajectory optimization and task offloading.
- 4) We evaluate the performance of the proposed mobility prediction model and DRL algorithm. Real-word traces and simulation results demonstrate that the proposed methods are superior in both effective mobility prediction and optimizations on task offloading and UAV flight trajectory compared with the existing benchmarks.

The organization of this paper is as follows. In Section II, the system model is introduced and the multi-stage optimization problem is formulated. Section III presents the hierarchical multi-scale Transformer framework for mobility prediction. Section IV provides the prediction-enhanced UAV trajectory optimization and task offloading algorithm. Performance evaluation results are shown in Section V. Finally, Section VI concludes our work and points out possible future work.

II. SYSTEM MODEL

We consider a UAV-enabled WBAN edge computing system as illustrated in Fig. 1, where a UAV equipped with an edge server has a mission to provides the proximate computation service for mobile WBAN users. The set of WBAN users is denoted as $\mathcal{U} = \{1, \dots, U\}$ and each user has N heterogeneous computation tasks from its equipped biosensors, indexed as $n \in \mathcal{N} = \{1, \dots, N\}$. The mission period of UAV is denoted as T^{\max} , which is slotted into T time slots, represented as $t \in \mathcal{T} = \{1, \dots, T\}$, with time slot duration of τ . Considering a 3-D Cartesian coordinate system, user $u \in \mathcal{U}$ has a zero altitude and its horizontal location at time slot t is denoted as

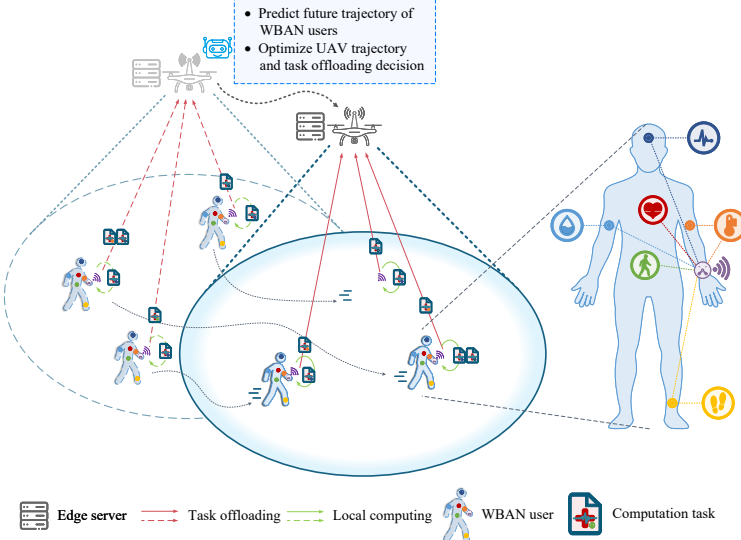


Fig. 1: System model

$\mathbf{p}_u[t] = (x_u[t], y_u[t])$. We assume the UAV flies at a fixed altitude H , and the initial horizontal locations of the UAV is preset as $\mathbf{p}_v[1] = (x_I, y_I)$. At the beginning of each time slot, WBAN users generate tasks and the UAV moves to the next location based on the observed locations and predicted user mobility. After relocating a new location of the UAV, WBAN users offload a portion of tasks via wireless links, and the UAV assists the execution of these computation tasks. At time slot t , the horizontal location of the UAV is denoted as $\mathbf{p}_v[t] = (x[t], y[t])$. It is assumed that the UAV flies with a constant speed $v[t]$ at time t and the direction of flight is represented by $\sigma[t]$. Then, the UAV flying from the previous hover location to the new location can be expressed as

$$\mathbf{p}_v[t + 1] = [x[t] + v[t]t^{\text{fly}} \cos \sigma[t], y[t] + v[t]t^{\text{fly}} \sin \sigma[t]], \quad (1)$$

where t^{fly} is the UAV flying time in each time slot.

A. Computation Task Model

Due to the varying sensed physiological states by each biosensor, the tasks of WBAN users are dynamically changed across time slots. For WBAN user u , its computation task n at time slot t is represented as a tuple $\Theta_{u,n}[t] = \langle I_{u,n}[t], D_{u,n}[t], C_{u,n}[t] \rangle$, where $I_{u,n}[t]$ is the current criticality

index of task n , $D_{u,n}[t]$ is the data load of task n , and $C_{u,n}[t]$ the computation amount of task n .

Specifically, criticality index $I_{u,n}[t]$ is comprised of three parts, ϕ_u , $\rho_{u,n}$ and $\alpha_{u,n}[t]$, where ϕ_u and $\rho_{u,n}$ are introduced to model the criticality of WBAN user u and its biosensor n , and $\alpha_{u,n}[t]$ represents the importance of the sensing data of biosensor n [26]. The larger the values of ϕ_u and $\rho_{u,n}$, the higher the data criticality of the corresponding user and its biosensor. For example, the data for heart disease patients have a higher criticality than healthy users, and the value of $\rho_{u,n}$ for ECG biosensor used to monitor heart is greater than that of EMG biosensor used to monitor muscle activity. Besides, the data of the same biosensor can be divided into normal data and emergency abnormal data. The data importance of biosensor $\alpha_{u,n}[t]$ indicates that the urgency of the sensing typical data $\theta_{u,n}[t]$. The predefined normal value range is $[\check{\theta}_{u,n}, \hat{\theta}_{u,n}]$. Without loss of generality, $\alpha_{u,n}[t]$ is classified as two levels, i.e., low and high. If $\theta_{u,n}[t]$ is within the predefined normal value range $[\check{\theta}_{u,n}, \hat{\theta}_{u,n}]$, it indicates the low urgency. Otherwise, it represents an abnormal states with high urgency. Thus, $\alpha_{u,n}[t]$ can be expressed as

$$\alpha_{u,n}[t] = \begin{cases} \text{low, if } \theta_{u,n}[t] \in [\check{\theta}_{u,n}, \hat{\theta}_{u,n}], \\ \text{high, if } \theta_{u,n}[t] \in (-\infty, \check{\theta}_{u,n}) \cup (\hat{\theta}_{u,n}, +\infty). \end{cases} \quad (2)$$

By jointly considering the user categories, biosensor categories and data importance, criticality index $I_{u,n}[t]$ of biosensor n for WBAN user u is defined as a function of the three factors, written as $I_{u,n}[t] = \mathcal{F}(\phi_u, \rho_{u,n}, \alpha_{u,n}[t])$.

Each task is atomically indivisible and can be processed locally or offloaded to the UAV for computing. Let $z_{u,n}[t] \in \{0, 1\}$ denote as the indicator of the task offloading decision for task $\Theta_{u,n}[t]$. $z_{u,n}[t] = 0$ signifies that task $\Theta_{u,n}[t]$ is computed at local hub node (e.g. a mobile device), and $z_{u,n}[t] = 1$ otherwise. Multiple tasks dispatched to the local hub node can be executed in parallel. Considering the distinct criticality of these locally-processed tasks, the local computation capability allocated to a task is proportional to the criticality index of the task. Define V_u as the local computation capability of WBAN user u , the computation resources allocated to task $\Theta_{u,n}[t]$

is denoted as

$$f_{u,n}^{\text{loc}}[t] = \frac{I_{u,n}[t]V_u}{\sum_{n \in \mathcal{N}} (1 - z_{u,n}[t])I_{u,n}[t]}. \quad (3)$$

Hence, the latency of local computing for task $\Theta_{u,n}[t]$ is then represented as

$$T_{u,n}^{\text{loc}}[t] = \frac{C_{u,n}[t]}{f_{u,n}^{\text{loc}}[t]}. \quad (4)$$

B. Task Offloading Model

For task offloading, both the effect of line-of-sight (LoS) and non-line-of-sight (NLoS) on wireless channel are taken into account in this work. Specifically, the probabilistic LoS model is adopted to model the large-scale attenuation between the UAV and WBAN users [27]. The probability of geometrical LoS between the UAV and each WBAN user depends on the statistical parameters related to the environment and the elevation angle. At time slot t , the LoS probability for user u is denoted as

$$\mathbb{P}^{\text{LoS}}(\beta_u[t]) = \frac{1}{1 + a \exp(-b(\beta_u[t] - a))}, \quad (5)$$

where a and b are environment-related parameters, and $\beta_u[t]$ is the elevation angle, represented as

$$\beta_u[t] = \frac{180}{\pi} \arctan \left(\frac{H}{\mathbf{p}_u[t] - \mathbf{p}_v[t]} \right). \quad (6)$$

Then, the non-line-of-sight (NLoS) channel probability is represented as $\mathbb{P}^{\text{NLoS}}(\beta_u[t]) = 1 - \mathbb{P}^{\text{LoS}}(\beta_u[t])$. Therefore, the expected channel gain is

$$g_u[t] = \frac{\mathbb{P}^{\text{LoS}}(\beta_u[t])g_0}{d_u^\varsigma[t]} + \frac{1 - \mathbb{P}^{\text{LoS}}(\beta_u[t])\kappa g_0}{d_u^\varsigma[t]}, \quad (7)$$

where $d_u^\varsigma[t] = \sqrt{H^2 + \|\mathbf{p}_u[t] - \mathbf{p}_v[t]\|^2}$ is the distance between WBAN user u and the UAV at time slot t , κ is the NLOS attenuation, g_0 is the channel gain at the reference distance d_0 and ς is the path loss exponent.

To prevent the signal interference among WBAN users, the frequency bands are orthogonally allocated to users. The wireless bandwidth available for user u is W_u Hz. When delivering the

tasks to the UAV for edge execution at time slot t , WBAN user u further assigns its bandwidth and transmission power $P_u[t]$ to its tasks according to the task criticality index. Let N_0 be the noise power at the UAV, then the transmission rate for offloading task $\Theta_{u,n}[t]$ can be obtained as

$$R_{u,n}[t] = \frac{I_{u,n}[t]W_u}{\sum_{n \in \mathcal{N}} z_{u,n}[t]I_{u,n}[t]} \log_2 \left(1 + \frac{I_{u,n}[t]P_u[t]g_u[t]}{\sum_{n \in \mathcal{N}} z_{u,n}[t]I_{u,n}[t]N_0} \right) \quad (8)$$

The data transmission time for $\Theta_{u,n}[t]$ is expressed as

$$T_{u,n}^{\text{trans}}[t] = \frac{D_{u,n}[t]}{R_{u,n}[t]}. \quad (9)$$

C. UAV Energy Consumption Model

During flight, the energy consumption of the UAV is mainly comprised of the propulsion energy consumption and the computation energy consumption. According to the existing analytical model for helicopter dynamics [13], its propulsion energy consumption at time slot t can be denoted as

$$E^{\text{fly}}[t] = \left(\gamma_1 v^3[t] + \frac{\gamma_2}{v[t]} \right) t^{\text{fly}}. \quad (10)$$

where γ_1 and γ_2 are parameters related to the weight, wing area, wing span efficiency of the UAV and air density, etc.

To improve the computation energy efficiency for offloaded tasks, a dynamic voltage and frequency scaling (DVFS) technique is leveraged by the UAV. By adjusting the CPU frequency of the UAV during each time slot, its computation power can be adaptively controlled. Let F_v denote as the total CPU frequency of the UAV. We consider the offloaded tasks of all WBAN users are executed concurrently by the UAV, and the computation capability allocated to an offloaded task is determined by the proportion of its criticality index to the total criticality index of all the offloaded tasks. Thus, the CPU frequency allocated to task $\Theta_{u,n}[t]$ is

$$f_{u,n}^{\text{uav}}[t] = \frac{I_{u,n}[t]F_v}{\sum_{u \in \mathcal{U}} \sum_{n \in \mathcal{N}} z_{u,n}[t]I_{u,n}[t]}. \quad (11)$$

Then, the computation time of task $\Theta_{u,n}[t]$ can be obtained as

$$T_{u,n}^{\text{comp}}[t] = \frac{C_{u,n}[t]}{f_{u,n}^{\text{uav}}[t]} = \frac{C_{u,n}[t] \sum_{u \in \mathcal{U}} \sum_{n \in \mathcal{N}} z_{u,n}[t] I_{u,n}[t]}{I_{u,n}[t] F_v}, \quad (12)$$

According to [28], the power consumption for computing task $\Theta_{u,n}[t]$ is $\eta f_{u,n}^3[t]$, where η is the effective capacitance coefficient of the UAV, which depends on its processor chip architecture. Thus, the energy consumption for computing task $\Theta_{u,n}[t]$ is represented as

$$E_{u,n}^{\text{comp}}[t] = \eta (f_{u,n}^{\text{uav}}[t])^2 z_{u,n}[t] C_{u,n}[t], = \frac{\eta z_{u,n}[t] C_{u,n}[t] I_{u,n}^2[t] F_v^2}{\left(\sum_{u \in \mathcal{U}} \sum_{n \in \mathcal{N}} z_{u,n}[t] I_{u,n}[t] \right)^2}. \quad (13)$$

D. Problem Formulation

To comprehensively measure the completion time gain of tasks with different criticality in each time slot, we define a weighted task completion time for each task based on its criticality index, as follows:

$$\Psi_{u,n}[t] = \frac{I_{u,n}[t]}{\sum_{u \in \mathcal{U}} \sum_{n \in \mathcal{N}} I_{u,n}[t]} T_{u,n}^{\text{total}}[t], \quad (14)$$

where $T_{u,n}^{\text{total}}[t]$ is the overall completion latency of task $\Theta_{u,n}[t]$, obtained as

$$T_{u,n}^{\text{total}}[t] = (1 - z_{u,n}[t]) T_{u,n}^{\text{loc}}[t] + z_{u,n}[t] (T_{u,n}^{\text{trans}}[t] + T_{u,n}^{\text{comp}}[t]). \quad (15)$$

Note that it is mandatory that each task should be completed within a time slot duration. That is, constraint $T_{u,n}^{\text{total}}[t] \leq \tau$ holds.

In this paper, we consider to minimize the weighted average task completion time of all the WBAN users during the UAV's mission period, subject to the total energy consumption of the UAV. By jointly optimizing the UAV flying trajectory and the task offloading decisions, the problem is

formulated as

$$\max_{v[t], \sigma[t], z_{u,n}[t]} \frac{1}{T} \sum_{t=1}^T \sum_{u=1}^U \sum_{n=1}^N \Psi_{u,n}[t] \quad (16a)$$

$$\text{s.t. } \sum_{t=1}^T \left(E^{\text{fly}}[t] + \sum_{u=1}^U \sum_{n=1}^N E_{u,n}^{\text{comp}}[t] \right) \leq E^{\text{uav}}, \quad (16b)$$

$$0 \leq T_{u,n}^{\text{total}}[t] \leq \tau, \forall u \in \mathcal{U}, n \in \mathcal{N}, t \in \mathcal{T}, \quad (16c)$$

$$\|\mathbf{p}_v[t+1] - \mathbf{p}_v[t]\| \leq V^{\max} \tau, \forall t \in \mathcal{T}, \quad (16d)$$

$$\sigma[t] \in [0, 2\pi], \forall t \in \mathcal{T}, \quad (16e)$$

$$z_{u,n}[t] \in \{0, 1\}, \forall u \in \mathcal{U}, n \in \mathcal{N}, t \in \mathcal{T}. \quad (16f)$$

where constraint (16b) indicates that the total energy consumption of UAV for flying and task computation is limited to its battery energy. Constraint (16c) guarantees that task $\Theta_{u,n}[t]$ is completed within a time slot duration. The flying speed of the UAV $v[t] \in [0, V^{\max}]$ is guaranteed by constraint (16d), where V^{\max} is the maximum flight speed. Constraint (16e) imposes limits on the UAV's angle of movement, and constraint (16f) indicates the task offloading decision variables. Problem (16) is a multi-stage dynamic optimization problem. Its non-convex property and complex time-correlated constraint present significant challenges for problem solving. Traditional optimization algorithms often fall into the curse of dimensionality, and are hard to adapt to rapid changes in network states. To address these issues, we propose an embodied AI framework that integrates mobility prediction and DRL to solve it in the next section.

III. HIERARCHICAL TRANSFORMER TRAJECTORY PREDICTION MODEL

In this section, we propose a user trajectory prediction model based on a hierarchical multi-scale Transformer framework, to capture the temporal dependencies of user mobility on various time scales. Traditional Transformer model [29] has been shown to effectively capture the long-range dependencies between words within a sentence in context of natural language processing. Its great sequence modeling ability facilitates to capture the contextual information of user mobility, which will help improve trajectory prediction performance. However, user trajectory typically exhibits multiple patterns with different human activities, characterized by significant variations

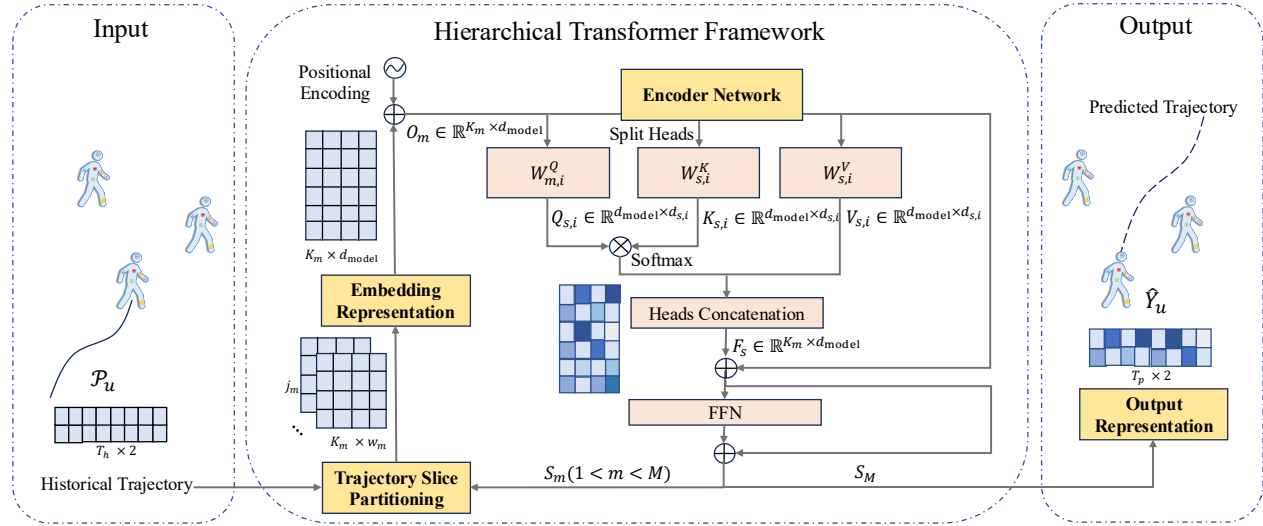


Fig. 2: Hierarchical Transformer Trajectory Prediction Model

and fluctuations across different temporal scales. Traditional transformer prediction model often analyze these patterns at a unified time scale, which can lead to inaccurate learning of mobility patterns. Hence, we develop a hierarchical transformer framework for learning multi-scale time series features of mobility patterns. In the following, a detailed overview of the hierarchical Transformer trajectory prediction model is provided.

The hierarchical Transformer trajectory prediction model is composed of four main modules: trajectory slice partitioning module, embedding representation module, encoder network module and output module. The overall structure of prediction model is illustrated in Fig. 2.

1) Trajectory Slice Partitioning: Suppose that the historical trajectory of user u is represented as $\mathcal{P}_u = \{p_u[1], \dots, p_u[T_h]\}$, with T_h as the length of the historical observation window. The whole hierarchical Transformer framework is divided into M stages that produce different feature maps of the historical trajectory for each user. To this end, a temporal slice partitioning strategy is designed to vary the time scale of the user trajectory at different stages. Specifically, a window slicing operation is leveraged to aggregate successive neighborhood location data, with the window slice size denoting the time scale size of the input. Let the user mobility trajectory sequence at stage $m \in \mathbb{R}$ denote by $S_m = [s_{m,1}, s_{m,2}, \dots, s_{m,n}]$, containing $n \in \mathbb{R}$ elements with dimensions of $j_m \in \mathbb{R}$. In particular, $S_1 = \mathcal{P}_u$ with $j_1 = 2$ denotes the raw user trajectory sequence of user u . The window slicing size at stage m is w_m , which means every w_m location data are grouped

into a new temporal trajectory slice. In this way, the trajectory sequence S_m input to stage m is partitioned into a set of fine-grained trajectory slices. The number of trajectory slices K_m and the size of each slice G_m are respectively denoted as:

$$K_m = \frac{|S_m|}{w_m}, \quad (17)$$

$$G_m = w_m \times j_m. \quad (18)$$

To some extent, it means that the length of the transformed trajectory sequence is K_m , and each trajectory data has feature dimension of G_m .

2) Embedding Representation: Through the embedding layer, these trajectory slices $S'_m \in \mathbb{R}^{K_m \times G_m}$ are projected into a higher dimensional space d_{model} . The embedding history feature $Z_m \in \mathbb{R}^{d_{\text{model}}}$ is denoted as

$$Z_m = \text{ReLU}(S'_m W_m^e + b_m^e), \quad (19)$$

where $\text{ReLU}(\cdot)$ [30] denotes the activation function, $W_m^e \in \mathbb{R}^{G_m \times d_{\text{model}}}$ is the embedding weight matrix and $b_m^e \in \mathbb{R}^{K_m \times d_{\text{model}}}$ is the bias term. To make the model understand the trajectory sequence order, locational encoding is also adopted to encode the relative locations of each data point within Z_m . Following [29], sine and cosine functions of different frequencies are used to implement the locational encoding, shown as below:

$$\begin{cases} \text{PE}_{\text{pos},2i} = \sin\left(\frac{\text{pos}}{10000^{2i/d_{\text{model}}}}\right), \\ \text{PE}_{\text{pos},2i+1} = \cos\left(\frac{\text{pos}}{10000^{2i/d_{\text{model}}}}\right), \end{cases} \quad (20)$$

where $\text{pos} \in \{1, 2, \dots, K_m\}$ is the location and $i \in \{1, 2, \dots, d_{\text{model}}/2\}$ is the dimension.

3) Encoder Network: The output $O_m \in \mathbb{R}^{K_m \times d_{\text{model}}}$ of the locational encoding are then processed using an encoder network. Specifically, O_m is firstly transformed to a query, a key and a value through different linear projections, as the inputs of the multi-head self-attention sublayer. The query can be regarded as the transformed matrix comprised of the feature vectors of each trajectory point in O_m , which is compared to the feature vectors of every other trajectory point in the key matrix. The relevance between a query and a key is computed by dot product. Define the query,

the key and the value of head i as $\mathbf{Q}_{m,i}$, $\mathbf{K}_{m,i}$ and $\mathbf{V}_{m,i}$, respectively. We have

$$\mathbf{Q}_{m,i} = \mathbf{O}_m \mathbf{W}_{m,i}^Q, \mathbf{K}_{m,i} = \mathbf{O}_m \mathbf{W}_{m,i}^K, \mathbf{V}_{m,i} = \mathbf{O}_m \mathbf{W}_{m,i}^V, \quad (21)$$

where $\mathbf{W}_{m,i}^Q \in \mathbb{R}^{d_{\text{model}} \times d_i}$, $\mathbf{W}_{m,i}^K \in \mathbb{R}^{d_{\text{model}} \times d_i}$, and $\mathbf{W}_{m,i}^V \in \mathbb{R}^{d_{\text{model}} \times d_i}$ are learnable projection parameters for head i at stage m , respectively. $d_i = d_{\text{model}}/h$ is the dimension of the feature vector of head i with h denoting the number of heads at stage m .

Then the output of the single head i at stage m is defined as:

$$\mathbf{A}_{m,i} = \text{softmax} \left(\frac{\mathbf{Q}_{m,i} \mathbf{K}_{m,i}^T}{\sqrt{d_i}} \right) \mathbf{V}_{m,i}. \quad (22)$$

Distinct attention heads are computed in parallel. Their outputs are then concatenated and projected to the dimension of d_{model} . The final output $\mathbf{F}_m \in \mathbb{R}^{K_m \times d_{\text{model}}}$ of the multi-head attention at stage m is as follows:

$$\mathbf{F}_m = [\mathbf{A}_{m,1}, \dots, \mathbf{A}_{m,h}] \mathbf{W}_m^O, \quad (23)$$

where $\mathbf{W}_m^O \in \mathbb{R}^{d_{\text{model}} \times d_{\text{model}}}$ is the weight parameter matrix of the linear projection at stage m .

The output of the self-attention sublayer is subsequently fed into a feed-forward neural network (FFN) sublayer, which consists of two linear transformations with a ReLU activation in between. Define \mathbf{W}_m^1 , \mathbf{W}_m^2 , \mathbf{b}_m^1 and \mathbf{b}_m^2 as learnable weights and bias of FFN at stage m , the process is described as:

$$\mathbf{F}'_m = \text{ReLU}(\mathbf{F}_m \mathbf{W}_m^1 + \mathbf{b}_m^1) \mathbf{W}_m^2 + \mathbf{b}_m^2. \quad (24)$$

Similar to the vanilla transformer encoder, these two sublayers are then enclosed within a residual connection to form an encoder layer that avoids the vanishing gradient problem. The overall encoder network is comprised of successive encoder layers, further enhancing the model's ability to learn complex patterns and dependencies in the user trajectory. The output \mathbf{F}'_m of the m -th stage is then as the input of the trajectory sequence \mathbf{S}_{m+1} for $(m+1)$ -th stage.

4) Output Representation: After the process of M stages, the output hidden representation of the final stage $\mathbf{F}'_M \in \mathbb{R}^{K_M \times d_{\text{model}}}$ from encoder network is flatten, and then the predicted trajectories

$\mathbf{Y}_u \in \mathbb{R}^{T_p \times 2}$ of user u is obtained through a linear projection, presented as

$$\hat{\mathbf{Y}}_u = [\text{Flatten}(\mathbf{F}'_M) \mathbf{W}^x + \mathbf{b}^x, \text{Flatten}(\mathbf{F}'_M) \mathbf{W}^y + \mathbf{b}^y], \quad (25)$$

where $\mathbf{W}^x, \mathbf{W}^y \in \mathbb{R}^{K_M d_{\text{model}} \times T_p}$ and $\mathbf{b}^x, \mathbf{b}^y \in \mathbb{R}^{K_M d_{\text{model}} \times T_p}$ denote the output weight matrix and bias vectors for 2-D coordinates of $\hat{\mathbf{Y}}_u$, respectively. T_p is the predicted horizon.

To evaluate the accuracy of the predicted trajectories generated by the hierarchical multi-scale Transformer, the root-mean-squared error (RMSE) is employed as the evaluation metric. RMSE measures the average Euclidean distance between predicted and ground truth locations across the prediction horizon. It is defined as

$$\mathcal{L} = \sqrt{\frac{1}{T_p} \sum_{t=1}^{T_p} \|\hat{\mathbf{Y}}_u - \mathbf{Y}_u\|}. \quad (26)$$

In training phase, the hierarchical Transformer trajectory prediction model is trained by minimizing the above RMSE.

IV. PREDICTION-ENHANCED UAV TRAJECTORY OPTIMIZATION AND TASK OFFLOADING ALGORITHM

In this section, the UAV agent makes decisions on its flight action and task offloading decisions at each time slot with the observed and predicted trajectory information of WBAN users. The Markov decision process (MDP) framework is firstly used to model problem (16) for the UAV edge computing network, and then a prediction-enhanced DRL algorithm for UAV trajectory optimization and task offloading is proposed.

A. MDP Elements Formulation

In this work, the key components of MDP are designed as follows.

1) **State Space:** The state space captures the environment's information at each time slot t . For our framework, the state encompasses the currently observable parameters and the predicted future user trajectory information. We define the state at time slot t as

$$s[t] = \{\mathbf{I}[t], \mathbf{P}[t], \mathbf{p}_v[t], E^{\text{remain}}[t]\}. \quad (27)$$

Here, $\mathbf{I}[t] = \{I_{u,n}[t]\}_{U \times N}$ is the set of task criticality index, $\mathbf{P}[t] = \{p_u[t]\}_{U \times 1}$ is the set of current user locations, $\mathbf{p}_v[t]$ is the UAV location and $E^{\text{remain}}[t] = E^{\text{remain}}[t-1] - \left(E^{\text{fly}}[t] + \sum_{u=1}^U \sum_{n=1}^N E_{u,n}^{\text{comp}}[t] \right)$ is the remaining energy of the UAV at time slot t . Particularly, at $t = 1$, $E^{\text{remain}}[t] = E^{\text{uav}}$. Thus, the dimension of the state space is $U(N + 1) + 3$.

2) Action Space: The action space represents the decisions made by the embodied UAV agent given a state. The selection of actions is based on the agent's policy, which is gradually optimized throughout the learning process. Specifically, the actions include the flying speed of the UAV, the flying angle of the UAV, and the task offloading decisions. The action taken by the agent at time slot t can be represented as

$$a[t] = \{v[t], \sigma[t], z_{u,n}[t]\}. \quad (28)$$

Note that $v[t] \in [0, v^{\max}]$ and $\sigma[t] \in [0, 2\pi]$ should be satisfied. For the task offloading decisions, we round it to the nearest integer in the range $[0, 1]$. That is, if $z_{u,n}[t] \in [0, 0.5)$, we have $z_{u,n}[t] = 0$; if $z_{u,n}[t] \in [0.5, 1]$, then $z_{u,n}[t] = 1$. The dimension of the action space is $UN + 2$.

3) Reward: The reward $r[t]$ evaluates the utility of the agent's action $a[t]$ at the given the state $s[t]$. In our algorithm, the reward function is designed to guide the UAV agent toward optimal actions by maximizing the task completion remaining time while considering the constraints on UAV energy consumption and task completion time. It is defined as

$$r(t) = \sum_{n \in \mathcal{N}} I_{u,n}[t](\tau - T_{u,n}^{\text{total}}[t]) \times \Omega^{\text{uav}} \times \Omega^{\text{time}}, \quad (29)$$

where Ω^{uav} and Ω^{time} are binary penalty terms that ensure the fulfillment of constraints (16b) and (16c), respectively. These penalty variables are defined as follows:

$$\Omega^{\text{uav}} = \begin{cases} 1, & \text{if } E^{\text{remain}}[t] \geq 0, \\ 0, & \text{if } E^{\text{remain}}[t] < 0. \end{cases}, \quad \Omega^{\text{time}} = \begin{cases} 1, & \text{if } T_{u,n}^{\text{total}}[t] \leq \tau, \\ 0, & \text{if } T_{u,n}^{\text{total}}[t] > \tau. \end{cases} \quad (30)$$

The reward function is strictly positive only when all constraints in problem (16) are satisfied.

B. Algorithm Design

In this work, proximal policy optimization (PPO), a representative reinforcement learning algorithm that has shown stable performance when implemented in various environments [31], is utilized to implement the prediction-enhanced UAV trajectory optimization and task offloading strategy. PPO is a policy gradient method within the actor-critic framework, where the actor network (parameterized by δ_A) defines the flight and offloading policy, and the critic network (parameterized by δ_C) estimates the value function. It is improved from the trust region policy optimization (TRPO) algorithm. TRPO constrains the distance between policies by Kullback-Leibler (KL) divergence, preventing an excessively large policy update in a single update. However, the computations using Taylor expansion approximations or conjugate gradients is overly complex. PPO, on the other hand, directly constrains the distance between the old policy $\pi_{\delta_A}^{\text{old}}$ and new policy π_{δ_A} within the objective function through the clipping method. The clipped version of the objective function is as follows:

$$L^{\text{CLIP}}(\delta_A) = \mathbb{E}_t \left[\min \left(\varphi_t(\delta_A) \hat{A}[t], \text{clip}(\varphi_t(\delta_A), 1 - \varepsilon, 1 + \varepsilon) \hat{A}[t] \right) \right], \quad (31)$$

where ε is a hyper-parameter that limits the update magnitude. $\varphi_t(\delta_A) = \pi_{\delta_A}(a[t]|s[t])/\pi_{\delta_A}^{\text{old}}(a[t]|s[t])$ represents the probability ratio between the new and old policies, and $\hat{A}[t]$ is the generalized advantage estimation at time t , which is calculated as

$$\hat{A}[t] = \sum_{l=0}^{\infty} (\gamma \lambda)^l (r[t+l] + \gamma V(s[t+l+1]) - V(s[t+l])), \quad (32)$$

where $V(s[t]) = \sum_{l=0}^{\infty} (\gamma)^l r[t+l]$ is the cumulative discounted reward, which also represents the state-value function. Following that, the loss function is defined as

$$L^C(\delta_C) = \frac{1}{2} \mathbb{E}_t \left[(V_{\delta_C}(s[t]) - V_{\text{tar}}(s[t]))^2 \right], \quad (33)$$

where $V_{\delta_C}(s[t])$ is the value calculated by the value network with hyper-parameters set δ_C , and $V_{\delta_C}(s_t)$ is the target value, i.e.,

$$V_{\text{tar}}(s[t]) = r[t] + \gamma V_{\delta_C}(s[t+1]). \quad (34)$$

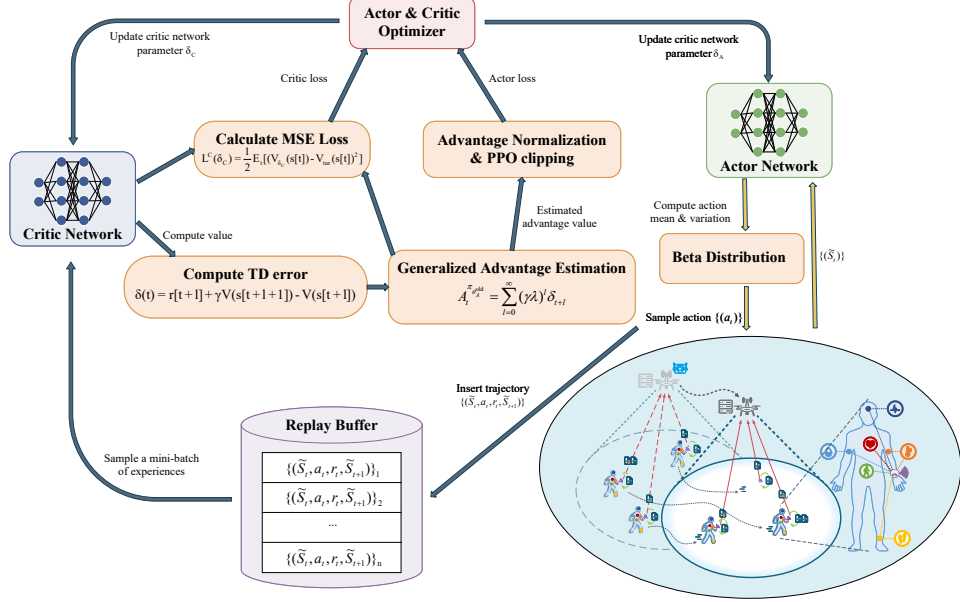


Fig. 3: The workflow of the interaction between the embodied UAV agent and the environment

Consequently, the actor and critic can be updated according to (31) and (33), respectively.

It is noted that the actions are typically continuous and bounded in this work. Conventional action sampling from Gaussian distribution by actor network will unavoidably introduce an estimation bias of policy gradient, since the boundary effects will be imposed by clipping the values of out-of-bound actions. To tackle this problem, we adopt Beta distribution instead of Gaussian distribution for the parameter learning of the actor network, which has the following form

$$f(x; \alpha_0, \beta_0) = \frac{\Gamma(\alpha_0 + \beta_0)}{\Gamma(\alpha_0)\Gamma(\beta_0)} x^{\alpha_0-1} (1-x)^{\beta_0-1}, x \in [0, 1], \quad (35)$$

where α_0 and β_0 are the parameters of Beta distribution. Since (35) has a bounded domain, it is appropriate to sample bounded actions. For a clear representation of the interaction between the embodied UAV agent and environment in our proposed method, we provide the detailed workflow in Fig. 3.

We then propose the UAV trajectory optimization and task offloading algorithm that integrates with user mobility information, shown as in Algorithm 1. In the training process of the algorithm, the UAV agent applies the trained hierarchical multi-scale Transformer model in Section III to predict the future mobility of WBAN users. Specifically, the UAV agent observes the current

Algorithm 1: Prediction-enhanced UAV Trajectory Optimization and Task Offloading Algorithm

```

1: Initialization: set the maximum episode  $E^{\max}$ , the maximum number of steps per episode  $T^{\max}$ , discount factor  $\gamma$ , hyper-parameter  $\varepsilon$ , learning rate, actor network  $\delta_A$ , critic network  $\delta_C$ , and create environment;
2: for  $e = 1 : E^{\max}$  do
3:   Reset the environment and obtain the initial state;
4:   for  $t = 1 : T^{\max}$  do
5:     Observe the current state  $s[t] = \{\mathbf{I}[t], \mathbf{P}[t], \mathbf{p}_v[t], E^{\text{remain}}[t]\}$ ;
6:     for Each WBAN user  $u \in \mathcal{U}$  do
7:       Predict user location  $\mathcal{P}_u[t] = \{\mathbf{p}_u[t+1], \dots, \mathbf{p}_u[t+T_p]\}$  based on the proposed mobility prediction model;
8:     end for
9:     Concatenate  $s[t]$  with  $\{\mathcal{P}_u[t]\}_{\mathcal{U}}$  to obtain integrated states  $\tilde{s}[t]$ ;
10:    Select action  $a[t]$  using the actor network based on policy  $\pi_{\delta_A}$  and get reward  $r(t)$ ;
11:    Based on  $s[t+1]$ , predict user location  $\mathcal{P}_u[t+1] = \{\mathbf{p}_u[t+2], \dots, \mathbf{p}_u[t+T_p+1]\}$  for each user and obtain integrated states  $\tilde{s}[t+1]$ ;
12:    Record the transition tuple  $(\tilde{s}[t], a[t], r[t], \tilde{s}[t+1])$  into the experience replay buffer;
13:    Sample random mini-batch of transitions from the experience replay buffer;
14:    Update actor network  $\delta_A$  via gradient descent on  $L^{\text{CLIP}}(\delta_A)$ ;
15:    Update critic network  $\delta_C$  by minimizing  $L^C(\delta_C)$  ;
16:    Update the state of the environment.
17:  end for
18: end for
  
```

state $s[t]$ from environment at time slot t . Based on the historical location information $\mathcal{P}_u[t] = \{\mathbf{p}_u[t-T_h+1], \dots, \mathbf{p}_u[t]\}$, the user mobility prediction algorithm is invoked to predict user location information $\{\mathbf{p}_u[t+1], \dots, \mathbf{p}_u[t+T_p]\}$ for each user u . This information is concatenated into the environment states. The integrated states $\tilde{s}[t]$ are used for the algorithm training. Then, actions are selected based on the actor network. The next state $s[t+1]$ is also integrated with the predicted location information to generate $\tilde{s}[t+1]$. Then, the experience samples are stored in the replay buffer with the rewards feedback from environment, and the actor and critic networks are updated using gradient descent to continuously optimize the UAV trajectory and task offloading policy.

V. PERFORMANCE EVALUATION

This section presents a comprehensive evaluation of the proposed hierarchical Transformer trajectory prediction model and the PETO algorithm. Specifically, we introduce the experimental dataset and simulation setting in subsection V-A. Then, we conduct testing and validation to

TABLE I: Environmental Parameter Settings

| Description | Value |
|---|----------------------|
| Altitude of UAV | 100m [32] |
| Mission Period T^{\max} | 100s [33] |
| Data load $D_{u,n}[t]$ | [1,2]MB |
| Computation amount $C_{u,n}[t]$ | [1,2] Gigacycles |
| Local computation capability V_u of user u | 1 Gigacycles/s [33] |
| Edge computation capability F_v of UAV d_{model} | 10 Gigacycles/s [33] |
| Channel bandwidth W_u for user u | 1MHz |
| Parameters of LOS channel a,b | 10, 0.6 [27] |
| NLOS attenuation κ | 0.2 [34] |
| Path loss exponent ς | 2.3 [34] |
| Channel gain at reference distance g_0 | 1.42e-4 [35] |
| Initial Energy E^{UAV} of UAV | 500kJ [36] |
| Effective capacitance coefficient η | 1e-27 [33] |
| Maximum flying speed V^{\max} | 50m/s [36] |
| Transmission power $P_u[t]$ | 100mW [37] |
| Noise Power N_0 | -60dBm [13] |

assess the performance of the trajectory prediction model in subsection V-B, while subsection V-C presents the simulation results for PETO algorithm in terms of weighted task completion time compared to baseline methods.

A. Experiment Setting

To evaluate the performance of the proposed trajectory prediction model, a real-world public human trajectory dataset is used for training and testing. The trajectory dataset was collected in the GeoLife project by Microsoft Research Asia [38]. The dataset contains precise latitude and longitude information on the consecutive locations of 182 users obtained from the GPS timestamp. The frame rate we adopt is 1s. For the trajectory data with intermittent missing values, we apply linear interpolation between adjacent observations. Each user trajectory is split into multiple segments with duration of $T_h + T_p$ seconds by window sliding, and use the data of last T_h seconds to predict the user's trajectory in the next T_p seconds. For training, validation and testing, the data set is divided in a 7:2:1 ratio.

TABLE II: Parameters in the Proposed Methods

| Description | Value |
|--|-------|
| Length of historical trajectory T_h | 60s |
| Length of predicted trajectory T_p | 10s |
| Number of stages M | 3 |
| Trajectory slice size w_m | 2 |
| Hidden size of the output d_{model} | 64 |
| Number of encoders | 6 |
| Batch size | 64 |
| Learning rate | 1e-3 |
| Clipping parameter ε | 0.2 |
| Hidden size of the actor/critic network | 128 |
| Discount factor γ | 0.98 |
| Replay buffer size | 1e6 |

For the performance evaluation on PETO algorithm, we then consider an environment containing 10 mobile WBAN users that generate tasks with different criticality. According to the 802.15.6 protocol [39], the services provided by the WBAN can be divided into four categories: non-medical services, low-priority medical services, general health services, and high-priority medical services. Each BAN user is equipped with five different physiological sensors to monitor data with different criticality, including background information, voice, ECG, body temperature, and movement, and generates corresponding data analysis tasks. Therefore, $\phi_u \in [0.25, 0.5, 0.75, 1]$, and $\rho_{u,n} \in [0.2, 0.4, 0.6, 0.8, 1]$ after normalization. The urgency of the perceived data is divided into normal data and emergency abnormal data, i.e., $\alpha_{u,n} \in [0.5, 1]$. Criticality index $I_{u,n}[t]$ is defined as $(\phi_u + \rho_{u,n} + \alpha_{u,n})/3$. The criticality of the data at different time slots follows the Markov property, and the corresponding state transition probability matrix is $[0.7, 0.3; 0.3, 0.7]$ [40]. To facilitate the distance computation between UAV and users, user locations are converted from the World Geodetic System coordinates to the Cartesian coordinate system by Haversine formula. Each time slot is divided into 1s of movement time and 1s of offloading and computation time [41]. Unless otherwise stated, the detailed environmental parameters are listed in TABLE I. For the implementation details of our hierarchical Transformer trajectory prediction model and the PETO algorithm, the default parameters are listed in TABLE II. Adam optimizer and standard

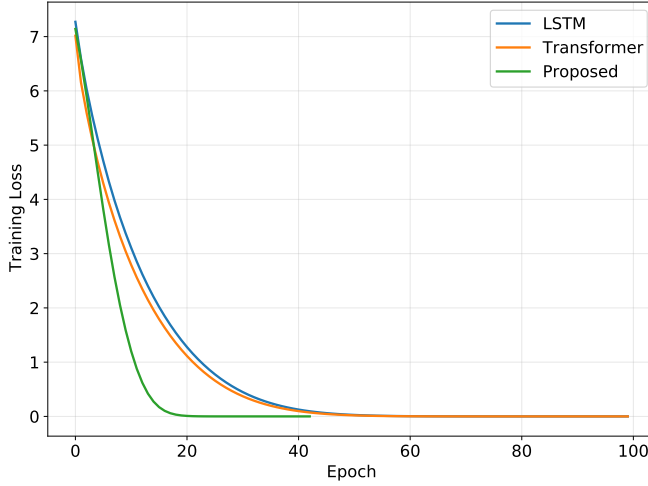


Fig. 4: Convergence behavior of mobility prediction models

normalization are employed for model training in both of the methods. To mitigate overfitting, we employ early stopping during training. Specifically, we monitor the validation loss and halt the training process if it does not decrease for 10 consecutive epochs, restoring the model parameters that achieved the best validation performance. In addition, all the experiments are implemented with PyTorch 1.13 [42] with Python 3.8 and trained on a T4 with 2560 CUDA cores.

B. Evaluation of Trajectory Prediction Model

To verify the effectiveness of the proposed trajectory prediction model, two prediction methods in the existing work are also implemented for comparative analysis. Specifically, LSTM-based user trajectory prediction [22] serves as the baseline algorithm. In the model, the LSTM cell with size 128 is used. Following that, two fully connected layers with the activation functions ReLU are added. The vanilla Transformer is also utilized to predict the user trajectory [43], in which the number of encoders and the attention heads are the same to the proposed hierarchical Transformer trajectory prediction model. These algorithms are repeated for 10 times with different seeds. The mean value of RMSE calculated using (26) from 10 experiments are reported.

Fig. 4 shows the convergence behavior of the three trajectory prediction models, in which their training loss are plotted with epochs. As epochs increases, the training loss of the three trajectory prediction models gradually decreases and approximately converges to 0. It can be observed that the proposed hierarchical Transformer trajectory prediction model exhibits more rapid convergence

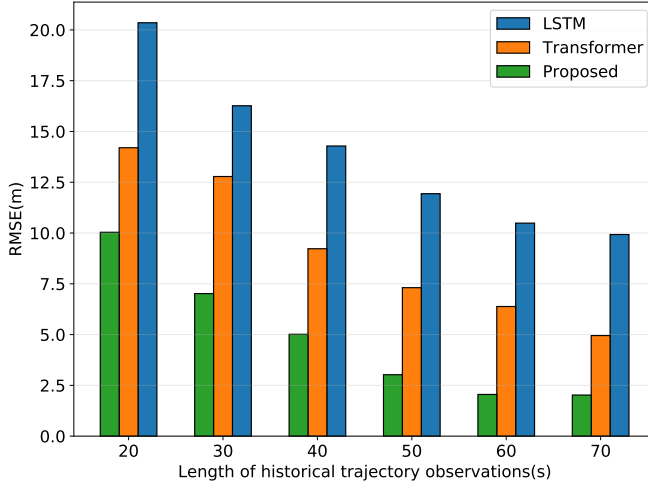


Fig. 5: RMSE comparison for user trajectory prediction models

compared to the other models, reaching a stable state approximately 20 epochs with early stopping triggered at epoch 42 to prevent overfitting.

To verify the prediction performance of different user trajectory prediction models, Fig. 5 presents their RMSE results on predicted trajectories against the actual ones over the historical observations from 20s to 70s. The predicted horizon is set to 10s. As shown in the figure, a longer historical observation windows contributes to more accurate predictions, in spite of the higher complexity. The improvement gap become small with the increasing length of historical observations. For the proposed hierarchical Transformer trajectory prediction model, the historical observations of 60s are enough for a good balance between accuracy and complexity. Compared to the LSTM model, both the two Transformer-based models achieve lower RMSE, particularly when the historical observation is long. Notably, the proposed hierarchical Transformer trajectory prediction model reduces RMSE by an average of 67.86%, with the most pronounced drop of 80.42% at 60s. This suggests that the multi-head self-attention attention mechanism in vanilla Transformer model and the proposed model can better capture long-range temporal dependencies in the user trajectory, which provides better mobility prediction. Besides, it can be observed that the proposed trajectory prediction model outperforms the vanilla Transformer model with fixed-scale feature representation, showing a consistent RMSE reduction with an average of 46.82%. This demonstrates the hierarchical feature extraction from small-scale fine-grained temporal trajectory

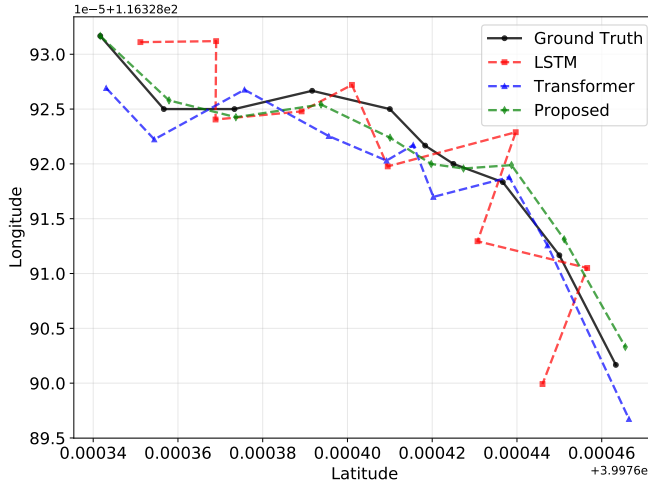


Fig. 6: Trajectory prediction results of different models

features to large-scale coarse-grained trajectory features is more effective for prediction.

In addition to quantitative metrics, the trajectory prediction results of different models are visualized in Fig. 6. In the figure, the prediction results of a representative user (ID 20) is illustrated. The X-axis represents the latitude value, and the y-axis represents the longitude value. Both the units of the X-axis and Y-axis are decimal degree of World Geodetic System coordinates. It is noted that the trajectory obtained by the proposed hierarchical Transformer prediction model is closely aligned with the actual trajectory, which exhibits its superior fitting accuracy. This result highlights the model’s ability to capture complex temporal dependencies of user movements.

C. Evaluation of PETO Algorithm

In this subsection, we validate the performance of the proposed PETO algorithm. The convergence results and the optimized UAV trajectory are firstly provided. Then, we compare the PETO algorithm with the following benchmark and state-of-the-art methods:

- 1) Random UAV trajectory and edge computing (RUEC): At each time slot, the UAV agent randomly chooses the flying speed and angle, and all the tasks are offloaded to the UAV by each WBAN user. Each task $\Theta_{u,n}[t]$ is allocated computation resources according to their criticality index $I_{u,n}[t]$.
- 2) PPO-based UAV trajectory optimization and task offloading algorithm without prediction (PAWP) [44]: At each time slot, the UAV agent observes the current system state, based

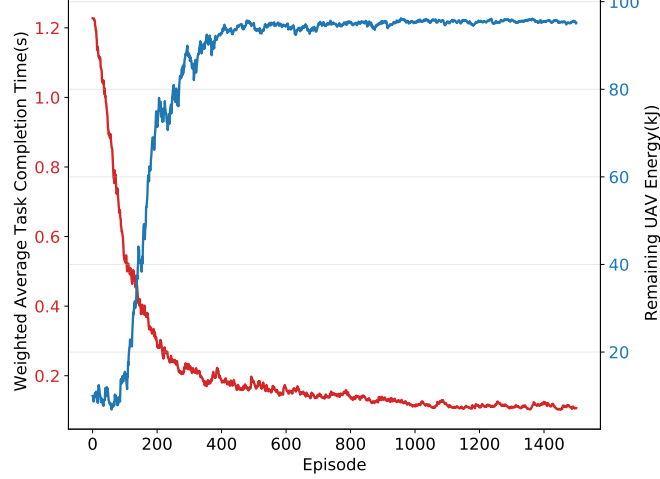


Fig. 7: Convergence behavior of the proposed PETO algorithm

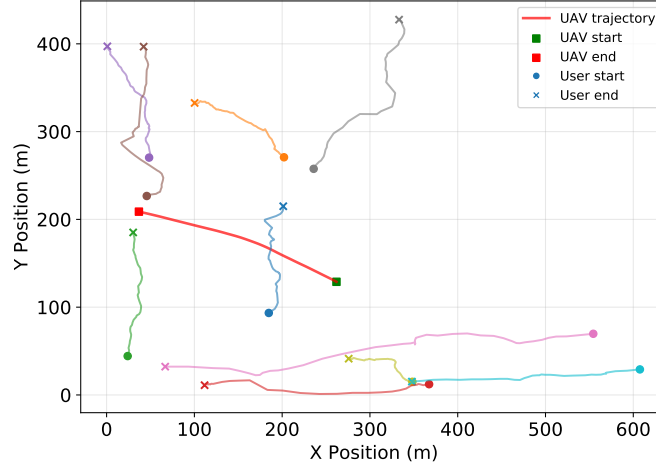


Fig. 8: UAV trajectory of the proposed PETO algorithm

on which the UAV agent optimizes trajectory and makes task offloading decisions by PPO reinforcement learning algorithm.

- 3) DDPG-based UAV trajectory optimization and task offloading algorithm with prediction (DAWP) [45]: At each time slot, the UAV agent utilizes the proposed trajectory model to predict the future user trajectory. According to the current state and the predicted partial state, the UAV agent optimizes trajectory and makes task offloading decisions by DDPG reinforcement learning algorithm.

Fig. 7 shows the convergence behavior of our PRTO algorithm, in which the weighted average task completion time and the UAV remaining energy in each episode are plotted with the evolution

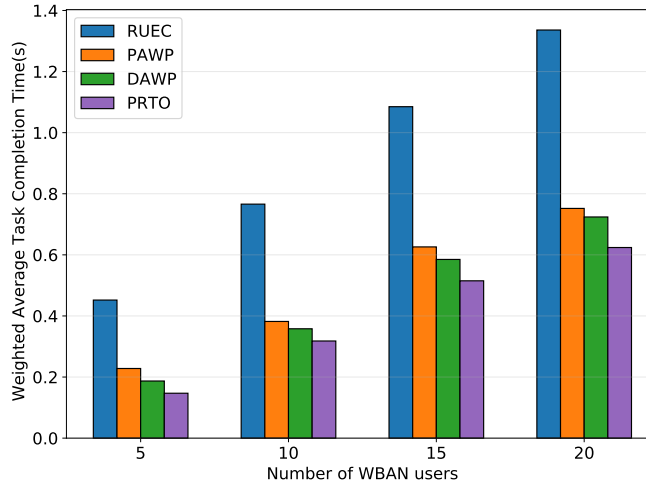


Fig. 9: Weighted average task completion time versus number of WBAN users

of episodes. In the early training stage, such as 0-1000 episodes, the PRTO algorithm still maintains a high exploration rate, causing the UAV agent to frequently try sub-optimal actions. As episode evolves, the weighted average task completion time declines and the UAV remaining energy grows as better trajectory and offloading strategies are learned from the environment dynamics, leading to more satisfactory performance. The results indicate that our PRTO method has stable convergence behavior and is reliable in this dynamic network environment. In addition, Fig. 8 characterizes both the users' trajectory and the designed UAV trajectory by the proposed PETO algorithm. The initial position of the UAV is determined by the geometric center of the user locations. It can be observed that the UAV agent intelligently follows a learned optimal trajectory in response to the movements of WBAN users, thereby maintaining the quality of edge computing services.

In Fig. 9, the performance comparison on weighted average task completion time of different solutions are illustrated as the number of WBAN users varies. With the increasing number of WBAN users, more users compete the limited computation resources of UAV, and the computation resources allocated to each task decrease. As a result, the weighted average task completion time grows in all the four methods. Note that the increase in weighted average task completion time gradually become small for the PAWP, DAWP and the proposed PRTO methods, this is because the computational demands of tasks from more WBAN users (e.g., 20) exceed the afforded computational capability of the UAV, results in most of the tasks being processed locally. It

is observed the proposed PRTO method consistently achieves superior performance compared to the other methods. Specifically, the proposed PRTO achieves 57.95% decrease in weighted average task completion time over RUEC on average. The performance gain comes from better flight trajectory and offloading decisions through the interactive learning of the embodied UAV agent. Without parallel computing at the local device and the UAV, too much tasks from WBAN users overloads the UAV in the RUEC method, leading to longer average task completion time. Compared to the PAWP method, the proposed PRTO method demonstrates approximately 21.76% gain in weighted average task completion time reduction. This improvement is attributed to the advanced prediction of user mobility by the proposed hierarchical Transformer framework, which facilitates the UAV to relocate a better position at each time slot to provide the edge computing service. Compared to DAWP, PRTO method also has better performance, which benefits from the use of generalized advantage estimation in PRTO provides more accurate advantage estimation and more effective action learning. These results demonstrate the scalability of our PRTO method, as it maintains superior performance gains even as the network size grows.

VI. CONCLUSIONS

In this paper, we have proposed an embodied AI-enhanced IoMT edge computing framework, in which the UAV embodied AI agent serves as the edge server for mobile WBAN users with time-varying task criticality. By integrating the designed hierarchical Transformer model for user mobility prediction and DRL for UAV flight trajectory and task offloading decision-making, the proposed method can reduce task completion time and improve adaptability in dynamic IoMT environments. Real-word traces have demonstrated that our proposed user mobility prediction method consistently outperforms traditional methods in terms of convergence speed and the prediction accuracy. In addition, simulations results have shown the proposed DRL algorithm greatly improves the task completion time performance through prediction enhancement, validating the effectiveness of using embodied AI framework in IoMT edge computing scenario.

REFERENCES

- [1] N. Y. Philip, J. J. Rodrigues, H. Wang, S. J. Fong, and J. Chen, “Internet of Things for in-home health monitoring systems: Current advances, challenges and future directions,” *IEEE J. Sel. Areas Commun.*, vol. 39, no. 2, pp. 300–310, 2021.

- [2] S. Movassaghi, M. Abolhasan, J. Lipman, D. Smith, and A. Jamalipour, "Wireless body area networks: A survey," *IEEE Commun. Surv. Tutor.*, vol. 16, no. 3, pp. 1658–1686, 2014.
- [3] S. Mu, Y. Lu, R. Jiang, W. Chen, B. Ai, and D. Niyato, "Aoi-aware online transmission optimization for WBANs with unreliable information delivery," *IEEE Trans. Wireless Commun.*, DOI:10.1109/TWC.2025.3620434, 2025.
- [4] Z. Ning, P. Dong, X. Wang, X. Hu, L. Guo, B. Hu, Y. Guo, T. Qiu, and R. Y. Kwok, "Mobile edge computing enabled 5g health monitoring for Internet of medical things: A decentralized game theoretic approach," *IEEE J. Sel. Areas Commun.*, vol. 39, no. 2, pp. 463–478, 2020.
- [5] Y. Lu, S. Zhang, C. Liu, R. Zhang, B. Ai, D. Niyato, W. Ni, and X. Wang, "Agentic graph neural networks for wireless communications and networking towards edge general intelligence: A survey," *arXiv preprint arXiv:2508.08620*, 2025.
- [6] T. Zhu, L. Kuang, J. Daniels, P. Herrero, K. Li, and P. Georgiou, "IoMT-enabled real-time blood glucose prediction with deep learning and edge computing," *IEEE Internet Things J.*, vol. 10, no. 5, pp. 3706–3719, 2022.
- [7] M. A. Rahman and M. S. Hossain, "An Internet-of-medical-things-enabled edge computing framework for tackling COVID-19," *IEEE Internet Things J.*, vol. 8, no. 21, pp. 15 847–15 854, 2021.
- [8] W. Mao, Y. Lu, G. Pan, and B. Ai, "UAV-assisted communications in SAGIN-ISAC: Mobile user tracking and robust beamforming," *IEEE J. Sel. Areas Commun.*, vol. 43, no. 1, pp. 186–200, 2025.
- [9] Q. Hu, Y. Cai, G. Yu, Z. Qin, M. Zhao, and G. Y. Li, "Joint offloading and trajectory design for UAV-enabled mobile edge computing systems," *IEEE Internet Things J.*, vol. 6, no. 2, pp. 1879–1892, 2018.
- [10] F. Guo, H. Zhang, H. Ji, X. Li, and V. C. Leung, "Joint trajectory and computation offloading optimization for UAV-assisted MEC with NOMA," in *IEEE Conf. Comput. Commun. Workshops(INFOCOM WKSHPS)*, 2019, pp. 1–6.
- [11] C. Sun, W. Ni, and X. Wang, "Joint computation offloading and trajectory planning for UAV-assisted edge computing," *IEEE Trans. Wireless Commun.*, vol. 20, no. 8, pp. 5343–5358, 2021.
- [12] Z. Liu, J. Qi, Y. Shen, K. Ma, and X. Guan, "Maximizing energy efficiency in UAV-assisted NOMA-MEC networks," *IEEE Internet Things J.*, vol. 10, no. 24, pp. 22 208–22 222, 2023.
- [13] X. Hu, K.-K. Wong, K. Yang, and Z. Zheng, "UAV-assisted relaying and edge computing: Scheduling and trajectory optimization," *IEEE Trans. Wireless Commun.*, vol. 18, no. 10, pp. 4738–4752, 2019.
- [14] Z. Bai, Y. Lin, Y. Cao, and W. Wang, "Delay-aware cooperative task offloading for multi-UAV enabled edge-cloud computing," *IEEE Trans. Mob. Comput.*, vol. 23, no. 2, pp. 1034–1049, 2022.
- [15] R. Amer, W. Saad, and N. Marchetti, "Mobility in the sky: Performance and mobility analysis for cellular-connected UAVs," *IEEE Trans. on Commun.*, vol. 68, no. 5, pp. 3229–3246, 2020.
- [16] J. Wang, X. Zhou, H. Zhang, and D. Yuan, "Joint trajectory design and power allocation for UAV assisted network with user mobility," *IEEE Trans. Veh. Technol.*, vol. 72, no. 10, pp. 13 173–13 189, 2023.
- [17] X. Yan, X. Fang, C. Deng, and X. Wang, "Joint optimization of resource allocation and trajectory control for mobile group users in fixed-wing UAV-enabled wireless network," *IEEE Trans. Wireless Commun.*, vol. 23, no. 2, pp. 1608–1621, 2023.
- [18] B. Omoniwa, B. Galkin, and I. Dusparic, "Optimizing energy efficiency in UAV-assisted networks using deep reinforcement learning," *IEEE Wireless Commun. Lett.*, vol. 11, no. 8, pp. 1590–1594, 2022.
- [19] Z. Yang, S. Bi, and Y.-J. A. Zhang, "Dynamic trajectory and offloading control of UAV-enabled MEC under user mobility," in *IEEE Int. Conf. Commun. Workshops (ICC Workshops)*, 2021, pp. 1–6.

- [20] X. Liu, Y. Liu, Y. Chen, and L. Hanzo, “Trajectory design and power control for multi-UAV assisted wireless networks: A machine learning approach,” *IEEE Trans. Veh. Technol.*, vol. 68, no. 8, pp. 7957–7969, 2019.
- [21] Q. Wu, Y. Zhang, Z. Yang, and M. R. Shikh-Bahaei, “Deep learning for secure UAV swarm communication under malicious attacks,” *IEEE Trans. Wireless Commun.*, vol. 23, no. 10, pp. 14 879–14 894, 2024.
- [22] H. Ma, Z. Zhou, and X. Chen, “Leveraging the power of prediction: Predictive service placement for latency-sensitive mobile edge computing,” *IEEE Trans. Wireless Commun.*, vol. 19, no. 10, pp. 6454–6468, 2020.
- [23] C.-L. Wu, T.-C. Chiu, and C.-Y. Wang, “Mobility-aware deep reinforcement learning with seq2seq mobility prediction for offloading and allocation in edge computing,” *IEEE Trans. Mob. Comput.*, vol. 23, no. 6, pp. 6803–6819, 2023.
- [24] R. Zhang, C. Zhao, H. Du, D. Niyato, J. Wang, S. Sawadsitang, X. Shen, and D. I. Kim, “Embodied AI-enhanced vehicular networks: An integrated vision language models and reinforcement learning method,” *IEEE Trans. Mob. Comput.*, vol. 24, no. 11, pp. 11 494–11 510, 2025.
- [25] R. Zhang, H. Du, Y. Liu, D. Niyato, J. Kang, Z. Xiong, A. Jamalipour, and D. I. Kim, “Generative ai agents with large language model for satellite networks via a mixture of experts transmission,” *IEEE J. Sel. Areas Commun.*, vol. 42, no. 12, pp. 3581–3596, 2024.
- [26] Z. Askari, J. Abouei, M. Jaseemuddin, and A. Anpalagan, “Energy-efficient and real-time NOMA scheduling in IoMT-based three-tier WBANs,” *IEEE Internet Things J.*, vol. 8, no. 18, pp. 13 975–13 990, 2021.
- [27] Y. Zeng, J. Xu, and R. Zhang, “Energy minimization for wireless communication with rotary-wing UAV,” *IEEE Trans. Wireless Commun.*, vol. 18, no. 4, pp. 2329–2345, 2019.
- [28] J. Xu, L. Chen, and S. Ren, “Online learning for offloading and autoscaling in energy harvesting mobile edge computing,” *IEEE Trans. Cogn. Commun. Netw.*, vol. 3, no. 3, pp. 361–373, 2017.
- [29] A. Vaswani, N. Shazeer, N. Parmar, J. Uszkoreit, L. Jones, A. N. Gomez, Ł. Kaiser, and I. Polosukhin, “Attention is all you need,” *Adv. Neural Inf. Process. Syst.*, vol. 30, 2017.
- [30] I. Goodfellow, Y. Bengio, and A. Courville, *Deep learning*. MIT press, 2016.
- [31] J. Schulman, F. Wolski, P. Dhariwal, A. Radford, and O. Klimov, “Proximal policy optimization algorithms,” *arXiv preprint arXiv:1707.06347*, 2017.
- [32] X. Tang, K. Zhao, C. Shen, Q. Du, Y. Wang, D. Niyato, and Z. Han, “Deep graph reinforcement learning for UAV-enabled multi-user secure communications,” *IEEE Trans. Mob. Comput.*, vol. 24, no. 9, pp. 8780 – 8793, 2025.
- [33] W. Liu, B. Li, W. Xie, Y. Dai, and Z. Fei, “Energy efficient computation offloading in aerial edge networks with multi-agent cooperation,” *IEEE Trans. Wireless Commun.*, vol. 22, no. 9, pp. 5725–5739, 2023.
- [34] Z. Yang, S. Bi, and Y.-J. A. Zhang, “Online trajectory and resource optimization for stochastic UAV-enabled MEC systems,” *IEEE Trans. Wireless Commun.*, vol. 21, no. 7, pp. 5629–5643, 2022.
- [35] L. Wang, K. Wang, C. Pan, W. Xu, N. Aslam, and A. Nallanathan, “Deep reinforcement learning based dynamic trajectory control for UAV-assisted mobile edge computing,” *IEEE Trans. Mob. Comput.*, vol. 21, no. 10, pp. 3536–3550, 2021.
- [36] H. Chen, H. Cui, J. Wang, P. Cao, Y. He, and M. Guizani, “Computation offloading optimization for UAV-based cloud-edge collaborative task scheduling strategy,” *IEEE Trans. Cogn. Commun. Netw.*, 2025.
- [37] Q. Ren, S. Lin, Y. Cai, X. Deng, L. Kong, S. Mumtaz, and B. Ai, “Resource allocation and slicing strategy for multiple services co-existence in wireless train communication network,” *IEEE Trans. Wireless Commun.*, vol. 24, no. 1, pp. 401–414, 2025.

- [38] Y. Zheng, X. Xie, W.-Y. Ma *et al.*, “Geolife: A collaborative social networking service among user, location and trajectory.” *IEEE Data Eng. Bull.*, vol. 33, no. 2, pp. 32–39, 2010.
- [39] K. S. Kwak, S. Ullah, and N. Ullah, “An overview of ieee 802.15.6 standard,” in *Int. Symp. Appl. Sci. Biomed. Commun. Technol. (ISABEL)*, 2010, pp. 1–6.
- [40] X. Yuan, C. Li, Q. Ye, K. Zhang, N. Cheng, N. Zhang, and X. Shen, “Performance analysis of ieee 802.15.6-based coexisting mobile WBANs with prioritized traffic and dynamic interference,” *IEEE Trans. Wireless Commun.*, vol. 17, no. 8, pp. 5637–5652, 2018.
- [41] Z. Hu, Y. Yang, W. Gu, Y. Chen, and J. Huang, “DRL-based trajectory optimization and task offloading in hierarchical aerial MEC,” *IEEE Internet Things J.*, vol. 12, no. 3, pp. 3410–3423, 2024.
- [42] A. Paszke, S. Gross, F. Massa, A. Lerer, J. Bradbury, G. Chanan, T. Killeen, Z. Lin, N. Gimelshein, L. Antiga *et al.*, “Pytorch: An imperative style, high-performance deep learning library,” *Adv. Neural Inf. Process. Syst.*, vol. 32, 2019.
- [43] A. Najjar, “Pre-trained transformer uncovers meaningful patterns in human mobility data,” in *IEEE Int. Conf. Big Data (BigData)*, 2024, pp. 5819–5828.
- [44] Y. Wang, J. Farooq, and H. Ghazzai, “Joint positioning and computation offloading in multi-UAV MEC for low latency applications: A proximal policy optimization approach,” *IEEE Trans. Mob. Comput.*, vol. 24, no. 10, pp. 9584–9598, 2025.
- [45] Y. Wang, W. Fang, Y. Ding, and N. Xiong, “Computation offloading optimization for UAV-assisted mobile edge computing: A deep deterministic policy gradient approach,” *Wirel. Netw.*, vol. 27, no. 4, pp. 2991–3006, 2021.